Nanoparticle metrology of silica colloids and super-resolution studies using the ADOTA fluorophore

Hazel L Stewart[1], Philip Yip[1], Martin Rosenberg,[2] Thomas Just Sørensen[2], Bo W. Laursen,[2]Alex E. Knight,[3] and David J S Birch[1‡]

[1]The Photophysics Research Group. Centre for Molecular Nanometrology, University of Strathclyde, Department of Physics, SUPA, John Anderson Building, 107 Rottenrow, Glasgow, G4 0NG, UK
[2]Nano-Science Center and Department of Chemistry University of Copenhagen, Universitetsparken 5, DK2100 København Ø, Denmark.
[3]Biotechnology Group, National Physical Laboratory, Teddington, Middlesex, TW11 0LW, UK

‡corresponding author: djs.birch@strath.ac.uk

Abstract

We describe how a new fluorescent dye, methyl ADOTA (N-methyl-azadioxatriangulenium tetrafluoroborate), is an improvement on dyes reported previously for measuring silica nanoparticle size in sols using the decay of fluorescence anisotropy. Me(thyl)-ADOTA possesses the unusual combination of having a red emission and a long fluorescence lifetime of ~ 20 ns, leaving it better-placed to reveal particle sizes at the upper end of the 1-10 nm measurement range. For stable LUDOX colloids, Me-ADOTA is shown to offer higher measurement precision in ≤ $1/30^{th}$ of the measurement time required for dyes previously used. In measurement times of only ~ 20 mins nanoparticle radii for LUDOX SM-AS, AM and AS-40 of 4.6 ± 0.3 nm, 5.9 ± 0.2 nm and 11.1 ± 1.1 nm, are in good agreement with two of the manufacturer's values of 3.5 nm, 6 nm and 11 nm respectively. Unlike the Si-ADOTA (N-(4-(triethoxysilylethyl)urea-phenyl-) ADOTA tetrafluoroborate) derivative containing a reactive trimetoxysilane group, Me-ADOTA is shown to not induce aggregation of colloidal silica. Measurements on nanoparticles growing in an acidic silica hydrogel at pH 0.94, prior to the gel time of ~ 50 hr, reveals an average nanoparticle size up to ~ 6.3 nm, significantly larger than the 4.5 nm reported previously. The difference is most certainly due to the longer fluorescence lifetime of Me-ADOTA (~ 20 ns) revealing the presence of larger particles. Studies of growing silica clusters in an alcogel of tetraethyl orthosilicate (TEOS) were able to resolve a monotonically increasing average radius of 1.42 ± 0.10 nm to 1.81 ± 0.14 nm over a period of 48 hr. We have also assessed a carboxylic acid derivative of ADOTA (N-(3-carboxypropylene)-ADOTA tetrafluoroborate - Acid-ADOTA) using dSTORM super-resolution microscopy. Although demonstrating high photochemical stability and blinking, its lower brightness and relative propensity to aggregate limits Acid-ADOTA's use for dSTORM.

Keywords: fluorescence lifetime, fluorescence anisotropy, nanoparticle metrology, silica sol-gel, ADOTA, dSTORM, super-resolution microscopy.

1. Introduction

There is growing awareness of the environmental and health consequences that might be associated with the proliferation of nanoparticles, particularly those in the 1-10 nm range that can traverse cellular membranes. Hand-in-hand with this interest goes the search for improved methods of measuring nanoparticle size for research, the need for low cost, more portable and easy-to-use methods that would facilitate wider monitoring, and the need for internationally agreed standards. A recent European Commission report [1] on measurement methods for nanoparticles serves to underline the importance of the topic and provides a useful summary of the main techniques in current use such as light scattering, small angle x-ray scattering (SAX), small angle neutron scattering (SANS) and scanning and transmission electron microscopy (SEM and TEM respectively).

Fluorescence is a phenomenon that enables many aspects of measurement science [2], perhaps most notably in the life sciences, where fluorescence can be influenced by the nanometre distances and nanosecond timescales that are often characteristics of physiology. Fluorescence has also been shown to play a key role in important applications of many types of nanoparticles [3] including those of silica [4]. Here we expand on the role of fluorescence in the metrology of nanoparticles, an area that underpins many such applications.

Some years ago the Photophysics group at Strathclyde University introduced an alternative approach to conventional methods for measuring 1-10 nm nanoparticles dispersed in solution that are well-known to be quite challenging. This is based on measuring the decay of fluorescence anisotropy of dye bound to a nanoparticle undergoing Brownian rotation in colloidal suspension. It has been shown to be capable of ~ 0.1 nm resolution and yet is of lower cost and easier to use than SAX, SANS, SEM and TEM. So far this has proved quite successful using a range of both electrostatically and covalently attached dyes in studies of silica nanoparticles growing during the sol-gel process [5,6,7] and stable LUDOX colloids that can provide useful metrology standards [8]. The approach been applied by others to a wider range of problems such as surface binding [9,10].

Nevertheless, despite finding wider application the use of fluorescence anisotropy for nanoparticle metrology is still in the proving ground and there is undoubtedly a need for improved dyes for this purpose. Potential errors and limitations include the possibility of dye aggregating on the nanoparticle, as this can cause depolarization by means of energy transfer, fluorescence decay time of the dye restricting the upper limit of measurable rotational time, depolarization due to dye wobbling or translating on the nanoparticle reducing the dynamic range of anisotropy measurement, and photochemical change in the dye leading to a change in its fluorescence decay time. Also, when studying mass-produced industrial-grade nanoparticles such as silica colloids there is the effect of intrinsic fluorescence, which can be difficult to quantify, but which will undoubtedly hide the particle rotational information being sought. With the aim of addressing these points we report here the application of the methyl derivative of a new triangulenium dye azadioxatriangulenium (ADOTA) to fluorescence nanometrology. The ADOTA dye is a highly chemically stable carbenium dye with numerous applications [11]. It has a workable fluorescence yield (~ 0.4 in water [12]), is photochemically robust, emits towards the red (peaking at ~ 560 nm) thus minimising background fluorescence and Rayleigh scatter and has a long fluorescence lifetime (~ 20 ns). The NHS ester of ADOTA has previously been combined with fluorescence anisotropy to study antibody binding (anti-rabbit

Immunoglobulin G to rabbit Immunoglobulin G) with rotational correlation times up to ~ 90 ns and has been shown to have a high initial anisotropy (~0.38 in rigid media [13]). Other applications demonstrated include fluorescence-based glucose sensing [14] and gated detection [15].

Recently the aggregation of an acid form of ADOTA (N-(3-carboxypropylene) azadioxatriangulenium tetrafluoroborate) has been observed in silica [16], but here we use Me-ADOTA, and show that unlike other derivatives, such as the silane derivative (Si-ADOTA), which covalently binds to silica, dye aggregation and dye-induced colloid aggregation are avoided. We demonstrate the use of Me-ADOTA to measure stable silica nanoparticles in LUDOX colloids and growing silica nanoparticles in both hydrogels and alcogels.

As well as studying the ensemble fluorescence properties of some ADOTA derivatives we have studied more closely some of their properties that are relevant to nanoparticle metrology, such as susceptibility to aggregate and photobleaching through their single molecule behaviour using the super-resolution microscopy technique dSTORM (Direct Stochastic Optical Recombination Microscopy) [17, 18], a form of single-molecule localisation microscopy (SMLM). SMLM relies on estimating the position of a single fluorophore very accurately from an image of its point spread function, and requires the acquisition of many images of a sample, each showing only a small subset of the fluorophores. This requires that the fluorophores used have the ability to be "switched" on and off in some way, usually by some kind of stochastic photochemical process. In dSTORM, this can be achieved using a single intense laser which pushes fluorophores into the triplet state, which is then reduced to a long-lived reduced state by a thiol-containing reagent. The ideal fluorophore has a low duty ratio (so that samples can be labelled at high density) and a high brightness in the "on" state (which gives a better precision); unfortunately only a few fluorophores approach this requirement closely enough to be useful. Ideally it may be possible to use a single dye to track the whole silica sol to gel process, from the sol containing nanoparticles measured using fluorescence anisotropy, to a gel composed of strands of silica observed with super-resolution microscopy.

2. Theory and analysis of fluorescence anisotropy decay data

By recording vertically and horizontally polarized fluorescence decay curves, $I_{VV}(t)$ and $I_{VH}(t)$, orthogonal to vertically polarized excitation, a time-resolved anisotropy function R(t) can be generated to describe the depolarization of fluorescence due to Brownian rotation of the fluorophore [19] i.e.

$$R(t) = \frac{[I_{VV}\,(t) - GI_{VH}\,(t)]}{[I_{VV}\,(t) + 2GI_{VH}\,(t)]} \tag{1}$$

where $G = I_{HV}(t)/I_{HH}(t)$ corrects for the relative transmission efficiencies of the two emission polarizations and is determined for horizontal orientation of the excitation polarizer [20].

In order to analyse equation (1) we first fit the denominator (which is in fact the fluorescence decay) to the minimum number of decay components needed using non-linear least squares (NLLS) reconvolution of the instrumental pulse generated by the source using a chi-sq (χ^2) goodness of fit criterion. This yields the best fit fluorescence decay parameters τ_{f1}, τ_{f2}, τ_{f3}, etc. associated with the fluorescence impulse response had we been using a δ function for excitation. (For a recent review of the analysis of fluorescence anisotropy decay see [21]). As a rule of thumb $\chi^2 < 1.2$ is usually taken to be an acceptable fit to the fluorescence decay.

Secondly, again using NLLS reconvolution of the instrumental pulse, we fit the product $R(t) \times [I_{VV}(t)+2GI_{VH}(t)]$ to the difference data $I_{VV}(t)-GI_{VH}(t)$,where $I_{VV}(t)+2GI_{VH}(t)$ is now described by the fluorescence impulse response parameters τ_{f1}, τ_{f2}, τ_{f3}, etc and R(t) describes the rotational kinetics in terms of the minimum number of rotational correlation times and associated amplitudes needed to describe the difference data. In our case here we chose to fit the fluorescence decay over all the channels of decay including the background determined from before the decay. The difference data was fitted from the peak down.

The simplest case occurs for a spherical rigid rotor in an isotropic medium such as a solvent [19]. If all the dye is rigidly attached to the nanoparticle, the decay of R(t) describes fluorescence depolarization due to Brownian rotation of the nanoparticle according to:

$$R(t) = R_0 \exp\left(-\frac{t}{\tau_r}\right) \tag{2}$$

where R_0 is the initial anisotropy with a maximum value of 0.4 for one photon excitation [19,20]. In this case τ_r is the nanoparticle rotational correlation time described by the Stokes-Einstein equation:

$$\tau_r = \frac{\eta V}{kT} \tag{3}$$

where η is the microviscosity, T the temperature, k the Boltzmann constant and V the hydrodynamic volume $4\pi r_p^3/3$ prescribed by the nanoparticle as defined by the hydrodynamic radius of interest r_p where

$$r_p = \left(\frac{3kT\tau_r}{4\pi\eta}\right)^{1/3} \tag{4}$$

In the case where the dye partitions between being bound to the nanoparticle and freely rotating (figure 1) we have

$$R(t) = (1-f)R_0 \exp\left(-\frac{t}{\tau_{r1}}\right) + fR_0 \exp\left(-\frac{t}{\tau_{r2}}\right) \tag{5}$$

where f is interpreted as the fraction of fluorescence due to dye bound to silica nanoparticles rotating with a correlation time τ_{r2} and $1-f$ to dye molecules unbound in the colloid and rotating faster with a correlation time τ_{r1}. Determining τ_{r1} can be useful as, by knowing the dye radius, it gives the microviscosity from equation (4). If the dye is wobbling on the nanoparticle, τ_{r1} will describe the average of free dye experiencing the bulk water microviscosity and dye in the vicinal viscosity close to the nanoparticle. Hence closely bound dyes are to be preferred.

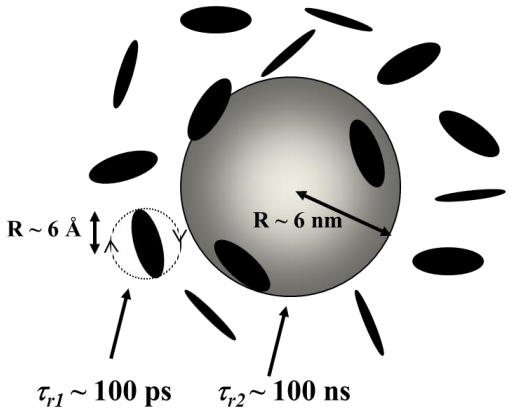

Figure 1. Dye bound to nanoparticle rotating with a correlation time τ_{r2} and co-existing with free dye characterized by a rotational correlation time τ_{r1}.

If dye molecules also bind to aggregates of the nanoparticles we can approximate this by:

$$R(t) = (1 - f - g)R_0 \exp\left(-\frac{t}{\tau_{r1}}\right) + fR_0 \exp\left(-\frac{t}{\tau_{r2}}\right) + gR_0 \quad (6)$$

where gR_0 describes a very slow rotation (defined by $\tau_{r2} >> \tau_f$), i.e. g is the fraction of fluorescence derived from dye attached to an aggregate of silica nanoparticles (or indeed a dye aggregate) such that negligible depolarization of fluorescence occurs during the fluorescence decay time. As pointed out by Weber many years ago [20] the ideal measurement condition for detecting maximum change in fluorescence anisotropy is when $\tau_r \sim \tau_f$ and of course this can never be realized for both τ_{r1} and τ_{r2} for a single dye in an anisotropy measurement. Nevertheless we have previously shown [8] that in many cases where a good estimate of the microviscosity is already known, by recording sufficient counts in the difference curve (the numerator in equation (1)) τ_r / τ_f ratios up to ~50 are possible. It is important to note that the difference between R_0 and the residual anisotropy gR_0 defines the useful dynamic range of anisotropy measurement in nanoparticle metrology.

Because it only concerns the hydrodynamic radius the above theory does not distinguish between solid nanoparticles and more ramified structure, both of which are encountered in the kinetics of the sol-gel formation of silica.

3. Methods and Materials

We have recently published a detailed description of the instrumentation and experimental protocols involved in using fluorescence anisotropy to measure nanoparticle size, including sample handling and spectroscopic characterization [22]. Here we provide a summary of these methods.

3.1 Fluorescence spectroscopy instrumentation

Fluorescence and anisotropy decay measurements were performed using time-correlated single-photon counting (TCSPC) [2] on a Horiba Scientific DeltaFlex system as shown in figure 2. The instrument incorporates wavelength selection by means of both excitation and emission monochromators, each with a Seya-Namioka geometry and holographic diffraction grating in order to minimise stray light. The instrument is similar to that used previously [7,8], but has been upgraded to include a 503 nm picosecond DeltaDiode operated at a higher repetition rate of 2 MHz (consistent with the 400 ns time range used) and faster DeltaHub data acquisition electronics with a dead time < 10 ns to accommodate this. Single fluorescence photons were detected using a TBX photon detection module incorporating a close-coupled power supply, amplifier and constant fraction discriminator. For anisotropy measurements the prism polarizer in the excitation channel remained at a vertical position during the measurements. The prism polarizer in the emission channel was then toggled automatically between vertical and horizontal positions for pre-set data acquisition times in order to record the two decay curves I_{VV} and I_{VH} independent of any source intensity fluctuation for use in equation (1). These measurements continued until a preset value in the

difference in counts between the peaks of I_{VV} and I_{VH} was achieved (10,000 was usually sufficient, but higher numbers were also evaluated). The G-factor in equation (1) was measured by setting the polarizer in the excitation channel to a horizontal position, and the polarizer on the emission channel arm rotated between vertical and horizontal positions to record G_{HV} and G_{HH}. Data analysis was performed using the Horiba Scientific DAS6 software package. Errors shown are 3 std. dev. unless stated otherwise.

Steady-state absorption measurements were performed on a Perkin-Elmer Lambda 2 spectrometer. Fluorescence spectra were recorded using a Horiba FluoroMax-2.

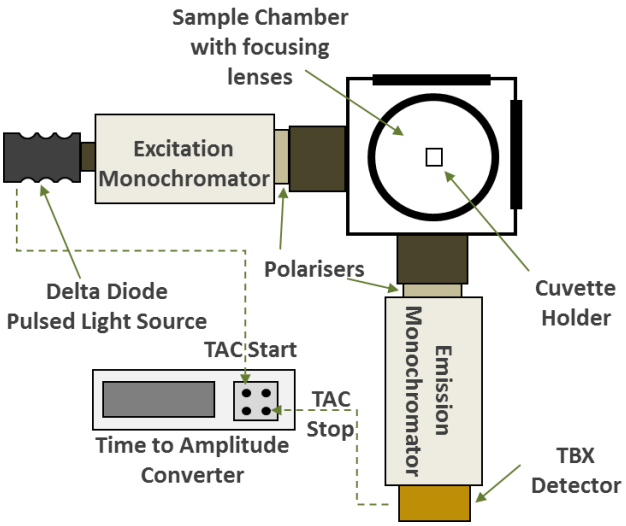

Figure 2. Schematic of the TCSPC fluorometer used to measure the fluorescence anisotropy decay.

3.2. Super-resolution microscopy

Direct stochastic optical reconstruction microscopy (dSTORM) measurements were performed using a custom-built total internal reflection fluorescence (TIRF) objective system based on an Olympus IX71 inverted microscope body with a UAPON 100XOTIRF objective. [18] Four lasers were used as excitation sources: a 640 nm Toptica Photonics IBEAM-SMART-640-S 150 mW, a 488 nm Coherent Sapphire 488-150 CW 150 mW, a 561 nm Coherent Sapphire 561-200 CW 200 mW and a 405 nm Mitsubishi ML320G2-11 150 mW (Laser Diode). The laser is focussed at the back focal plane of the microscope objective, and the position of the focus is controlled by a motorised mirror to enable adjustment of the angle of incidence. A quad-band dichroic mirror and emission filter are used to separate excitation and emission light, and a further filter wheel with band pass filters is used to avoid cross-talk. An Andor EMCCD iXon Ultra 897 camera was used for data acquisition. This camera was air cooled at –80 °C. It has 512×512 pixels, with a pixel size of 16×16 µm and a 16 bit digitisation. The resolution per pixel with the 100× objective is therefore 0.16×0.16 µm. Data acquisition was carried out using a LabView program written in-house and data analysis was carried out using the "rainSTORM" MATLAB GUI and ImageJ [23]. Samples were placed in Nunc Lab-Tek chambered cover glasses for imaging.

3.3. Materials and sample preparation

The ADOTA derivatives Me-ADOTA and Acid-ADOTA were synthesized as described previously [11]. Si-ADOTA (a reactive triethoxy silane derivative) was synthesized by similar methods. Rhodamine 6G (R6G) was obtained in pure form from Sigma-Aldrich. Figure 3 shows the structure of the dyes used.

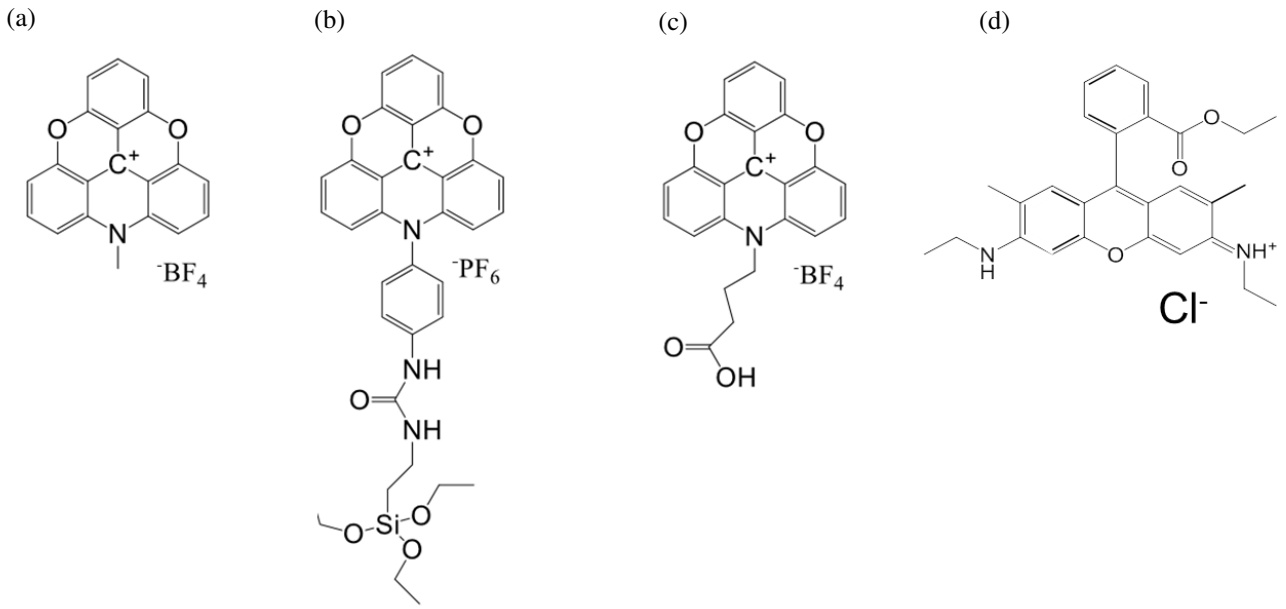

Figure 3. Dyes used in the study. (a) Me-ADOTA, (b) Si-ADOTA, (c) Acid-ADOTA (d) R6G, (d). Using equation (4) we have measured the hydrodynamic radius of Me-ADOTA to be ~ 0.61 nm in ethylene glycol and ~ 0.42 nm in glycerol i.e. comparable to ~ 0.56 nm for R6G [6].

In stock solutions each dye had an absorbance of ~ 0.1, which is appropriate for fluorescence anisotropy studies [22]. Where relevant doubly deionized water was used that was found to be free of background fluorescence and all samples were sealed with parafilm in 4 cm^3 plastic cuvettes, these having been previously shown to be free of strain-induced birefringent effects [7,8].

LUDOX colloidal silica (Grace) with radii that were studied previously [7,8] were chosen for comparison, covering radii of 3.5 nm, 6 nm and 11 nm for SM-AS, AM and AS-40 respectively. Each LUDOX sample has an associated pH stability range (typically ~ 9-10). Stabilised solutions consisting of water and either sodium hydroxide or ammonium hydroxide were made for each sample. SM-AS was measured at 0.1 % concentration and AM and AS-40 at a 2 % concentration in stabiliser solution.

Silica gel is usually manufactured on an industrial scale using hydrogels of sodium silicate. To study the growth of acidic silica hydrogel nanoparticles, samples were prepared using similar methods to those described previously [5] and adjusted as necessary to produce a suitable volume of solution with an appropriate gel time, thus enabling a direct comparison with our previous work using JA120 i.e. a different dye [5]. Typically, 11.39 mL of Crystal 79 sodium silicate solution (PQ Corporation) diluted to an 8.14 % concentration in water was added to 5.73 mL of

sulphuric acid at a 12 % concentration in water, giving a gel time of ~ 50 hr. The solution was mixed for 30 minutes and the initial pH was measured to be 0.94. The polymerization is triggered by the condensation of the mono silicic acid ($Si(OH)_4$) to form siloxane (– Si – O –Si –) monomeric structures that aggregate to form growing and ramified nanoparticles, which eventually span the containing vessel at a gel time t_g. Chemical reactions of the following type occur:

Hydrolysis: $$Na_2O \cdot xSiO_2 \cdot yH_2O + H_2SO_4 \rightarrow Si(OH)_4 + Na_2SO_4 \quad (7)$$

Condensation: $$Si(OH)_4 + Si(OH)_4 \rightarrow 2SiO_2 + 4H_2O \quad (8)$$

Where x and y relate to the fractions of silica and soda in the silicate precursor.

For laboratory work the higher purity and better defined structure of alcogels of orthosilicates compared to sodium silicate means they are usually preferred. Here we have used alcogels of tetraethyl orthosilicate (TEOS), where the equivalent hydrolysis reaction is:

Hydrolysis: $$Si(OC_2H_5)_4 + 4\ H_2O \rightarrow Si(OH)_4 + 4\ C_2H_5OH \quad (9)$$

This leads to similar condensation reactions as per equation (8).

The TEOS gel was prepared under acidic conditions as described previously [22]. Briefly, to prepare the gel 7.5 ml of TEOS was mixed with 7.75 ml of ethanol, and 9.5 ml of water was then added plus a few drops of hydrochloric acid to catalyse the reaction, followed by thorough mixing for 4 hr. t_g was ~ 70-90 hr.

The exact photochemistry and photophysics of dSTORM are likely to vary from dye to dye, but in a typical dye used for dSTORM the following model is believed to explain the blinking mechanism. The “on” state of the fluorophore corresponds to rapid cycling between the ground state and excited state with the emission of many photons. Although the probability of transitioning from the excited state to the triplet state is low, the rapid cycling induced by the intense illumination ensures this is achieved fairly rapidly. Once in the triplet state the molecule is reduced rapidly to a stable radical state. Depleting oxygen reduces the rate of oxidation of this radical state back to the ground state, “trapping” molecules in the dark state for long periods (ensuring a low “duty ratio”). It was not known previously whether ADOTA can exhibit this kind of behaviour.

The dSTORM buffer used consists of 3 stock solutions. A 50 µl of enzyme stock solution (A), 400 µl of glucose stock solution (B), 50-100 µl of MEA stock solution (C) is topped-up with PBS (450-500 µl). Enzyme stock solution A is made up of 100 µl of 1 g ml–1 of catalase, 200 µl of 1 M TCEP, 25 ml of glycerol, 22.5 ml of water, 1.25 ml of 1 M KCl, 1 ml of 1 M Tris-HCL (pH 7.5) and 50 mg of glucose oxidase. Glucose stock solution (B) is made up of 5 g of glucose, 5 ml of glycerol and 45 ml of water. MEA-Stock solution (C) is made up of 1136 mg of MEA-HCl in 10 ml of water. These are stored at –20 °C. Acid-ADOTA was prepared as a stock solution (~1 mg/ml) using DMF as a solvent. The dye was sonicated to ensure that it completely dissolved. 40 µl of this was mixed with 200 µl of 0.01 % 10,000 MW amino dextran and left to incubate for 15 minutes in a Lab-Tek Chamber.

After incubation the solution was pipetted off and then the chamber was filled with dSTORM buffer and sealed with a cover slip. A layer of Acid-ADOTA (Figure 3c) was used rather than Me-ADOTA in order to cross-link it to the dextran. The basis of the protocol used has been reported previously [24].

4. Results and Discussion

4.1. LUDOX nanoparticles

Some of the fluorophores used previously to label LUDOX [25,26], such as those based on 6-methoxyquinoline, have comparable fluorescence lifetimes to ADOTA, but suffer from requiring UV excitation. This has been shown to also excite intrinsic fluorescence in such colloids [8], thus introducing a source of error that is ever-present and difficult to quantify, but which is minimized and usually negligible by exciting red dyes such as Me-ADOTA. Indeed exciting all the LUDOX colloids at 503 nm revealed negligible intrinsic fluorescence. Figure 4 shows the absorption and fluorescence spectra for Me-ADOTA attached to LUDOX AM to have slight bathochromic shifts of 3 and 4 nm respectively. (This contrasts with the hypsochromic shift of fluorescence and bathochromic shift of absorption for 6-methoxyquinoline on LUDOX [8]). The fluorescence lifetime decay of Me-ADOTA in water was found to be described well by a mono-exponential of 19.4 $\pm$ 0.1 ns (χ^2 ~ 1.2). In colloidal silica (SM-AS) bi-exponential fluorescence decay components (χ^2 ~ 1.19) of 13.9 $\pm$ 0.3 ns (9.30 %) and 25.1 $\pm$ 0.2 ns (90.70 %) were found. The significant difference in decay time in water and in the presence of silica nanoparticles suggest the Me-ADOTA is comprehensively attached to the particle with negligible unbound.

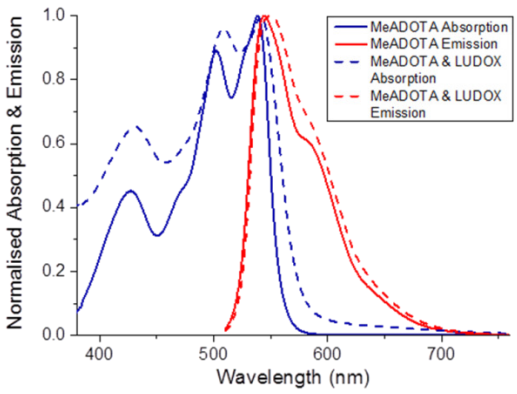

Figure 4. Absorption and fluorescence spectra of Me-ADOTA on LUDOX AM and in water.

Initially we sought to covalently label the LUDOX colloids using the reactive silane derivative of Si-ADOTA shown in figure 3b in the manner we had used previously for fluorescein bound to a methoxysilane [7]. This makes sense as it is expected to give a more strongly bound fluorescent label than with electrostatic binding, thus eliminating the possibility of dye wobbling on the nanoparticle surface introducing an additional rotational time. However, in this case we found the Si-ADOTA to aggregate the LUDOX rather than binding solely to the LUDOX. This is illustrated in the time-resolved fluorescence anisotropy measurement of figure 5(a) for AS-40, where the lack of depolarization suggests the Si-ADOTA-LUDOX aggregate is significantly larger than the 11 nm radius of AS-40 that is revealed in the Me-ADOTA measurement of figure 5(b).

(a) **(b)**

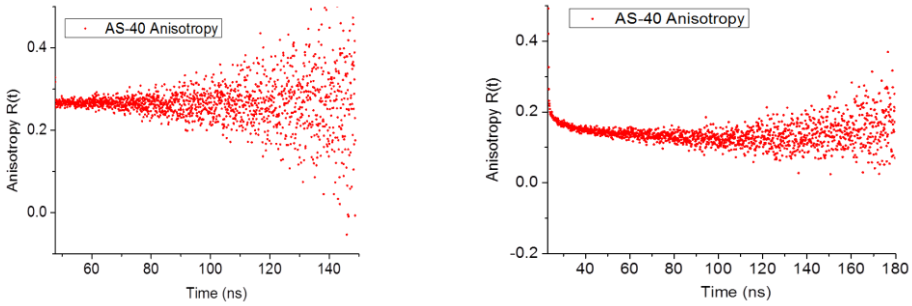

Figure 5. Time-resolved fluorescence anisotropy for LUDOX AS-40 colloid labelled with (a) Si-ADOTA and (b) Me-ADOTA. The incremental time channel width is 0.104 ns.

Table 1. Fluorescence anisotropy decay analysis of various LUDOX colloids obtained with Me-ADOTA using equations (4) and (5). The anisotropy data was acquired in typically ~ 20 min. The microviscosity was taken to be 10^{-3} Pa s (1 cp). The measured average particle radius r_p, the manufacturer's values r_m and the particle radii obtained previously using 6-methoxyquinoline [8] are shown. The latter were measured in ~ 10 hr with 10^5, $5x10^5$ and 10^6 counts in the peak D_p of the difference curve $I_{VV}(t) - GI_{VH}(t)$ for SM-30, AM-30 and AS-40 respectively, at a channel width of 28 ps, whereas only $\leq 10^4$ counts were required in D_p at a channel width of 104 ps for a better precision in $\mathbf{r_p}$ to be obtained with Me-ADOTA. Note: SM-AS and AM are denoted by the manufacturer has having the same size as SM-30 and AM-30 respectively, the only difference being the counter ion.

	Present work						**Previous work [8]**	
LUDOX	**$D_p/10^3$ (cts)**	**τ_{r1} (ns)**	**τ_{r2} (ns)**	**χ^2**	**r_p (nm)**	**r_m (nm)**	**r_p [8] (nm)**	**$D_p/10^5$ (cts)[8]**
SM-AS	3.0	3.48 ± 0.93	100.0 ± 18.0	1.18	4.6 ± 0.3	3.5	4.0 ± 0.4 (SM-30)	1.0
AM	3.5	4.08 ± 1.30	210 ± 19.5	1.09	5.9 ± 0.2	6.0	6.4 ± 0.5 (AM-30)	5.0
AS-40	12.0	12.1 ± 2.06	1424 ± 471	1.18	11.1 ± 1.1	11.0	11.0 ± 1.6 (AS-40)	10.0

Table 1 shows the agreement between typical measurements obtained using Me-ADOTA, the manufacturer's values and those we obtained previously are all within error apart from SM-AS where, as observed previously for the equivalent colloid SM-30 [8], small aggregates (binary, tertiary etc) of the colloid can occur with time as carbon dioxide entering the sample leads to lowering of pH and a higher average size. It is also interesting to speculate that the adherence of vicinal water might also play a part by increasing the hydrodynamic radius to a level that is more apparent in such smaller nanoparticles. However, it should be noted that when exciting the 6-methoxyquinolium dyes in the UV, the radii r_p (from our previous work [8] shown in table 1) required the collection of ~ 100x the number of counts (and proportionate increase in measurement time) to obtain the comparable precision afforded by Me-ADOTA. We attribute this advantage of Me-ADOTA to excitation at 503 nm obviating the effect of the

colloid's intrinsic fluorescence decay in masking the particle rotational information when labelling with UV dyes [8, 25, 26]. For comparison in table 2 we have increased the precision of measurement with Me-ADOTA by increasing the number of counts in the peak D_p of the difference function I_{VV} (t) – GI_{VH} (t) (eq. 1) simply by measuring for longer. Interestingly this makes little difference to the accuracy of the particle size measurement, but the higher precision is reflected in the reduced statistical error. Indeed the precision in radius is shown to be significantly better for Me-ADOTA than 6-methoxyquinolium dyes, even though the latter had for all the colloids a much higher count in D_p. The χ^2 values are larger in table 2 than for table 1. This is to be expected as the higher statistical precision can reveal small systematic errors such as scattered excitation, time-base non-linearity etc. No improvement in χ^2 was gained by including a third rotational time or residual anisotropy in order to describe larger aggregates as previously reported for some LUDOX samples [8].

Table 2. Fluorescence anisotropy decay analysis of LUDOX colloids measured with Me-ADOTA as per table 1, but with up to ~ 26 times more counts in the peak of the difference function D_p of equation (1)**.**

LUDOX	$D_p/10^3$ (cts)	τ_{r1} (ns)	1- fR_0 (%)	τ_{r2} (ns)	fR_0 (%)	χ^2	r_p (nm)	r_m (nm)
SM-AS	78	2.22 ± 0.17	3.86	78.0 ± 4.7	96.14	2.35	4.2 ± 0.1	3.5
AM	92	5.96 ± 0.53	0.83	216.0 ± 6.2	99.17	1.88	5.9 ± 0.1	6.0
AS-40	98	10.2 ± 1.92	0.16	1580 ± 342	99.84	3.96	11.5 ± 0.8	11.0

4.2. Hydrogels of sodium silicate

Acidic silica hydrogels were prepared under similar conditions to those described previously [5] for ease of comparison. We labelled two identical hydrogel compositions separately with Me-ADOTA and R6G in order to assess the effect of the difference in fluorescence lifetimes (Me-ADOTA ~ 20 ns, R6G ~ 4 ns) on the apparent particle size as polymerization proceeds according to equations (7) and (8). Unlike stable LUDOX colloids, in the case of a polymerizing hydrogel, the measurements need to be done as quickly as possible in order to minimise the size distribution of the particles being detected.

(a) **(b)**

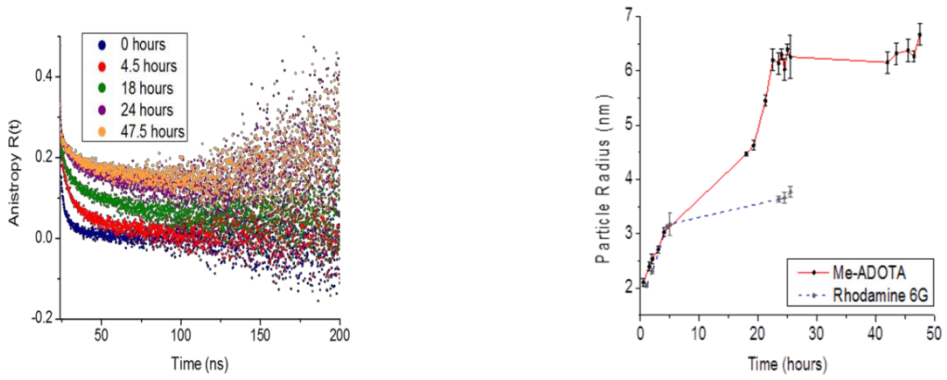

Figure 6. (a) Changes in fluorescence anisotropy for an acidic silica hydrogel at pH ~ 0.94 labelled with Me-ADOTA as polymerization proceeds. (b) Comparison of the apparent change in average particle radius determined using Me-ADOTA and R6G during the polymerization.

Figure 6(a) shows typical changes in the fluorescence anisotropy decay obtained using Me-ADOTA for a sol with a gel time t_g ~ 50 hr at initial pH ~ 0.94 and figure 6(b) compares the apparent average radii derived from such data for Me-ADOTA and R6G. The anisotropy data acquisition time at each time delay was ~ 20 mins. The longer fluorescence lifetime of Me-ADOTA clearly reveals the presence of larger particles (~ 6.3 nm) than those detected by R6G (~ 3.7 nm). In such acidic hydrogels the silica particles are thought to grow initially by monomer addition and then diffusion controlled cluster-cluster aggregation [5], and would not be expected to grow continuously below the gel point as silicate is progressively used up in the hydrolysis and condensation reactions of equations (7) and (8). With t_g ~ 50 hr the levelling of the particle growth after ~ 25 hr may well reflect this consumption of silicate. However, it is also possible that particles larger than ~ 6.3 nm are present, with the finite fluorescence lifetime decay of ADOTA limiting their detection in the 20 min measurement time used. Nevertheless, in our early work, where we introduced the idea that the rotation of dye attached to silica hydrogel nanoparticles explained the observed fluorescence anisotropy decay [5], we used the xanthene dye JA120 because it had the virtues of being excited at 650 nm, a peak fluorescence at ~ 690 nm and survived acidic conditions. However, the fluorescence lifetime of JA120 was only ~ 1.8 ns in water and this led to the maximum size detected of ~ 4.5 nm. The data of figure 6, obtained using Me-ADOTA, suggests that larger particles up to at least ~ 6.3 nm are indeed present, these being observable due to the longer fluorescence lifetime of Me-ADOTA as compared to that of JA120.

4.3 Alcogels of tetraethyl orthosilicate (TEOS)

The polymerization of orthosilicate alcogels proceeds through different aggregation kinetics to sodium silicate hydrogels. Under base-catalysed (alkaline, Stöber) conditions orthosilicate gelation proceeds more rapidly and less ramified, with more discrete nanoparticles of narrower defined size formed as compared to acidic conditions, where cross-linking of more linear structures is observed prior to gelation [27,28]. Under such Stöber conditions we recently used fluorescence anisotropy decay to demonstrate the control of silica nanoparticles size in the range of $\mathbf{r_p}$ ~ 3.1nm - 3.8 nm for TEOS [7]. Under acidic conditions for tetramethyl orthosilicate (TMOS) studied using R6G we earlier reported the slow growth of smaller silica structures from ~ 0.8 nm to 1.0 nm over several weeks [6].

Table 3. Fluorescence anisotropy decay analysis of Me-ADOTA in a TEOS sol under acidic conditions and analysed using equations (4) and (5).

Time (hr)	τ_{r1} (ns)	1- fR_0 (%)	τ_{r2} (ns)	fR_0 (%)	χ^2	r_p (nm)
19.0	0.20 ± 0.19	16.01	3.00 ± 0.70	83.99	1.11	1.42 ± 0.10
21.0	0.34 ± 0.09	18.54	3.14 ± 0.83	81.46	1.02	1.45 ± 0.12
23.0	0.43 ± 0.11	21.51	4.03 ± 1.45	78.49	1.04	1.57 ± 0.17
43.5	0.30 ± 0.12	12.93	4.07 ± 1.14	87.07	1.03	1.58 ± 0.14
46.5	0.32 ± 0.11	14.27	4.50 ± 1.10	85.73	1.04	1.63 ± 0.12
48.5	0.83 ± 0.19	23.40	6.00 ± 2.26	76.60	1.06	1.79 ± 0.20
67.0	0.50 ± 0.14	14.95	6.13 ± 1.59	85.05	0.98	1.81 ± 0.14

Table 3 shows the results of the anisotropy analysis of Me-ADOTA in TEOS under acidic conditions as described in section 3.3. Over 48 hr a monotonically increasing nanoparticle radius of ~ 1.4 nm to 1.8 nm, as determined from

τ_{r2}, is observed. This is consistent with the increased size of TEOS compared to TMOS [6]. Such measurements provide a stern test of the resolution of the technique and reveal close to 0.1 nm precision with $\mathbf{D_p}$ ~ 3,500 cts acquired in ~ 20 min. The τ_{r1} value of ~ 0.3 ns up to 46.5 hr is generally consistent with free dye rotation in water. The increasing τ_{r1} values around the gel time t_g (~ 70-90 h) are more indicative of dye wobbling when constrained within the vicinal water of more confined silica structures. It seems unlikely that changes in microviscosity η could account for the observed increase in r_p given the $r_p \sim \eta^{-1/3}$ power dependence in equation (4) and previous work showing [5, 6] η decreasing rather than increasing as the precursors species are consumed.

4.4 Super resolution studies of Acid-ADOTA-Dextran photostability and dye aggregation

In order to test the susceptibility to aggregation, photochemical robustness of the ADOTA fluorophore, and to see if it was suitable for tracking the whole sol-gel process from particle to gelation, we irradiated its acid derivative linked to dextran with laser excitation in order to populate dark states in the manner required for dSTORM measurements, and monitored the recovery of its fluorescence. The power dependence, that reflects the generation of dark states following increase in fluorescence, is shown in Figure 7 for Acid-ADOTA-Dextran (structure shown in figure 3(c)), which has also recently been used [29] to label and record the rotation of Bovine Serum Albumin using fluorescence anisotropy (τ_r ~ 37 ns).

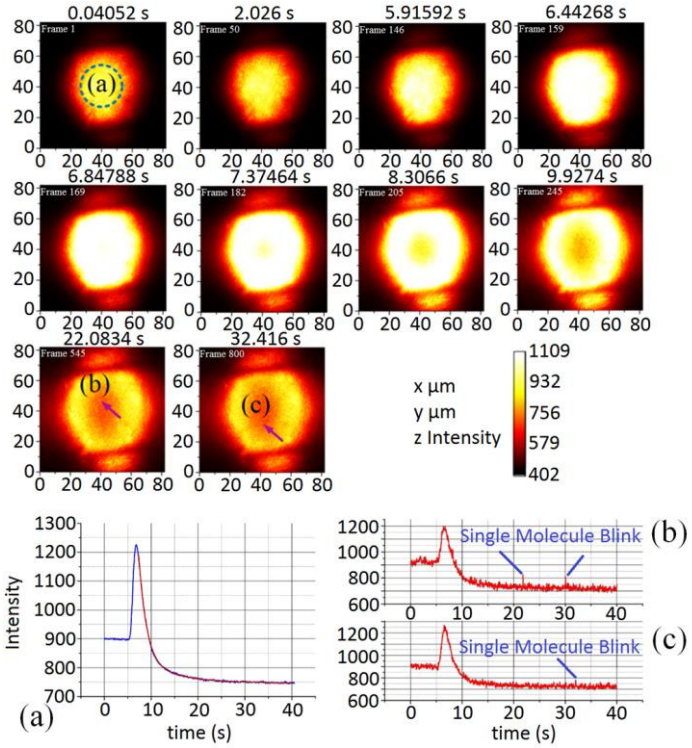

Figure 7. Objective TIRF image frames of the fluorescence from the Acid-ADOTA-Dextran layer. Axes in x and y are labelled in µm. The colour scale corresponds to the number of photons counted. The TIRF illumination footprint has a two-dimensional Gaussian profile; however because of the non-linear response the fluorescence intensity at the highest illumination is lower, giving a "doughnut" appearance. The intensity of the fluorescence increases with the increasing laser power as one might expect; however the intensity then decreases, following an approximate bi-exponential decay as the fluorophore switches into a photostable dark state. Initially at 5% laser power the two decay constants required to describe the fluorescence fall time in (a) above are 1.71 ± 0.01 s and 8.9

± 0.3 s. Arrows indicate the position of the intensity traces (b) and (c) that correspond to single molecule emissive blinks above the fluorescence background following depletion of the fluorescence due to the molecules entering dark states. The intensity of the 488 nm laser illumination was altered from t ~ 5 s to increase from 5 % to 90 % of the 150 mW maximum power using a rotating waveplate and a polariser. A band-pass filter at 525 nm with a 50 nm bandwidth was used for emission selection. Each frame (512 × 512 pixels) was acquired for 0.01 s and the cycle time was 0.04052 s.

Figure 7 shows selected microscope image frames at different time intervals as the laser power (488 nm, 150 mW) is ramped up from 5 % to 90 %. The fluorescence intensity from Acid-ADOTA-Dextran is seen to resemble the Gaussian shape of the laser when the power is maintained at 5 % (Frames 1 and 50). As the laser power is increased to 90 % (Frames 146, 159 and 169) the fluorescence intensity is seen to increase firstly at the central spot and then towards the edges until a continuous fluorescence intensity is observed (Frame 169). The central spot then stops fluorescing as the high laser power leads to the formation of the stabilised Acid-ADOTA-Dextran dye radical (Frame 182). The dark central spot of this doughnut increases in diameter (Frames 205, 245 and 545) while the edges of the doughnut which have less power than the central spot continue to fluoresce. Single molecule blinks (Frames 545 and 800) can be observed as brighter spots within the darker regions of fluorescence depletion in the microscopy images within the central doughnut. Figure 7(a) shows the average bulk intensity time profile over the central doughnut, and 7(b) is the average intensity profile over the pixels where the single molecule blink as observed in Frame 545 and 7(c), where the single molecule blink is observed in Frame 800.

Acid-ADOTA-Dextran was found to demonstrate excellent recovery of its native fluorescence properties following laser irradiation and in this regard is at least comparable to other dyes that have been assessed for SMLM [30]. This is illustrated in Figure 8.

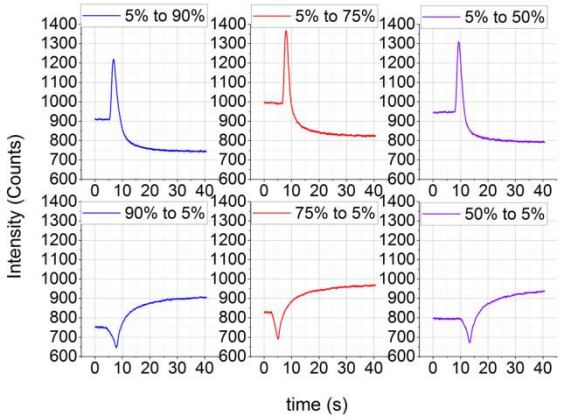

Figure 8. The effect fluorescence intensity (photon counts detected) as a function of time for Acid-ADOTA-Dextran when increasing and decreasing the laser power from 5 to 90 % and back down to 5 %, 5 to 75 % and back to 5 % and 5 to 50 % and back down to 5 % respectively. The dye fluorescence is shown to recover well to the original level, showing no evidence of bleaching. These curves correspond to integrated intensities over the central circle irradiated as shown in figure 7.

As can be seen in figures 7(b) and (c) the single molecule emission of Acid-ADOTA-Dextran is only just bright enough to be seen above the background and despite the photochemical robustness of the dye this currently limits

its use in dSTORM studies. Given that the fluorescence quantum yield of ADOTA is only ~ 2x lower (0.4 in water [12]) than the commonly used dyes for dSTORM, we associate the low brightness with the much lower extinction coefficient of ADOTA. For example for ADOTA this is 9480 M^{-1} cm^{-1} in Acetonitrile at 541 nm [13]. At the higher end of dye performance for dSTORM the extinction coefficient for ATTO 565 is 120,000 M^{-1} cm^{-1} and its quantum yield is 0.9 [30]. At the lower end, say for FITC, the extinction coefficient is 70,000 M^{-1} cm^{-1} at 494 nm and its quantum yield is 0.8 [30]. We chose 150 mW laser power for ease of comparison, as this is what we use for more typical dyes for dSTORM such as Alexa 647, Cy5 and Alexa 561. In the event we could have increased the laser power above the 150 mW in order to increase the proportion of dye molecules in the dark state, but this is never without unwanted effects such as bleaching and heating. Also, the long fluorescence lifetime of ADOTA (~ 20 ns), as compared to commonly use dyes for dSTORM (~ 1 ns), probably does not help depletion.

Moreover, under the higher concentrations needed for dSTORM (in contrast to the lower concentrations needed for nanoparticle metrology using anisotropy) we have observed some aggregation of the free Acid-ADOTA dye (i.e. when not bound to dextran) as illustrated in figure 9.

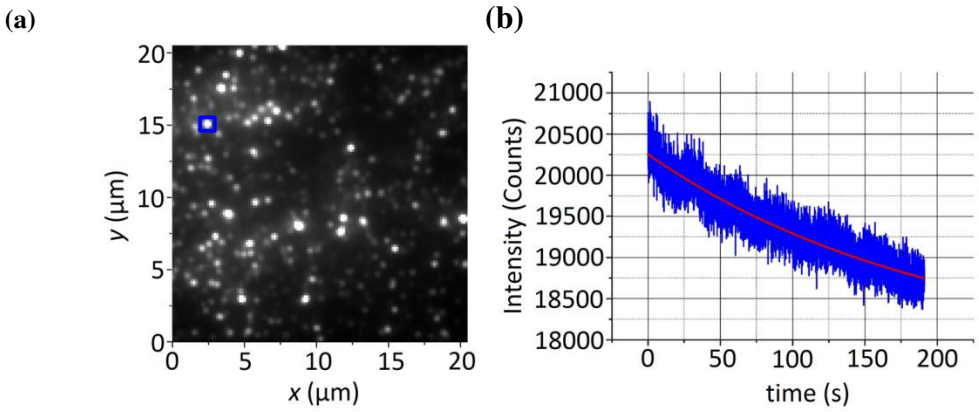

Figure 9. (a) The sum image of the free Acid-ADOTA (i.e. not linked to dextran) measured with a CCD capture rate of 0.01912 s for 10,000 frames. 128 pixels were used in both x and y at 160 nm/pixel with axes in x and y labelled in µm. (b) A typical bright object (framed in (a)) was examined in more detail. Its brightness was observed to decrease with respect to time and approximately fitted to an exponential decay of the form $y = A_1 \exp(-x/t_1) + y_0$ where $y_0 = 17800 \pm 50$, $A_1 = 2450 \pm 40$, $t_1 = 200 \pm 6$ s and the $R^2 = 0.879$.

Photobleaching or the switching of a single molecule would be expected to be a step function, not the exponential decay shown in figure 9(b). Indeed, the fact that an exponential decay is observed confirms the presence of aggregates of Acid-ADOTA when not bound to dextran. Results such as those shown in Figure 9 provide a useful test for aggregation. Such behaviour would be a detriment in nanoparticle metrology as it facilitates energy transfer (and consequentially a depolarization mechanism unrelated to particle rotational depolarization) and in tracing the assembly of silica structures using dSTORM. However, the silica nanoparticle studies on Me-ADOTA shown here do not demonstrate aggregation effects, and other bespoke derivatives of the ADOTA fluorophore may well be worthy of further investigation for use in SMLM.

Conclusions

For the range of particle sizes and pH encountered with silica, no one single dye structure is likely to be ideal for nanoparticle metrology using fluorescence anisotropy under all conditions of interest. However, Me-ADOTA has been shown to demonstrate a combination of critical characteristics that are useful in the study of both alkaline and acidic silica sols and no doubt other types of nanoparticles. These have extended the limits of measurement precision through the minimization of systematic errors such as having a fluorescence lifetime too short to measure nanoparticle size in a reasonable measurement time, exciting background fluorescence, Rayleigh scattered excitation and photochemical degradation. The fluorescence behaviour of dyes under dSTORM conditions is shown to offer a stringent test of dye photophysics that can inform the study of nanoparticles using fluorescence anisotropy decay. SMLM has already been shown to resolve temporal changes (e.g. [31]) on timescales comparable to silica gelation and further work is planned to resolve more closely nanoparticle silica structures by means of super-resolution microscopy, ideally using the same dye as used for anisotropy studies.

Acknowledgements

We would like to thank SFC for a SUPA INSPIRE research studentship for PY and PQ Corporation for their support.

References

[1] Linsinger T P J, Roebben G, Gilliland D, Calzolai L, Rossi F, Gibson N, Klein C 2012 Requirements on measurements for the implementation of the European Commission definition of the term “nanomaterial”. European Commission Joint Research Centre Report. doi 10.22787/63490

[2] Birch D J S, Chen Y and Rolinski O J 2015 Fluorescence Photonics: Scientific Foundations, Technology and Applications, Volume IV, Biological and Medical Photonics, Spectroscopy and Microscopy. Ed. D L Andrews. Wiley. **Ch.1**. 1-58.

[3] Demchenko A P 2013 Nanoparticles and nanocomposites for fluorescence sensing and imaging Methods Appl. Fluoresc. **1** 022001. doi:10.1088/2050-6120/1/2/022001

[4] Bonacchi S, Genovese D, Juris R, Montalti M, L Prodi, Rampazzo E and Zaccheroni N 2011 Luminescent silica nanoparticles: extending the frontiers of brightness Angewandte Chemie Int. Ed. **50**, 4056-4066.

[5] Birch D J S and Geddes C D 2000 Sol-gel particle growth studied using fluorescence anisotropy: an alternative to scattering techniques Phys. Rev. E **62** 2977–80

[6] Karolin J, Geddes C D, Wynne K and Birch D J S 2002 Nanoparticle metrology in sol-gels using multiphoton excited fluorescence Meas. Sci. Technol. **13** 21–7.

[7] Yip P, Karolin J and Birch D J S 2012 Fluorescence anisotropy metrology of electrostatically and covalently labelled silica nanoparticles. Meas. Sci. Technol. **23** 084003 (8 pages).

[8] Apperson K, Karolin J, Martin R W and Birch D J S 2009 Nanoparticle metrology standards based on the -resolved fluorescence anisotropy of silica colloids Meas. Sci. Technol. **20** 025310

[9] Tleugabulova D, Duft A M, Brook M A and Brennan J D 2004 Monitoring solute interactions with poly(ethylene oxide)-modified colloidal silica nanoparticles via fluorescence anisotropy decay Langmuir **20** 101-108

[10] Tleugabulova D, Zhang Z, Chen Y, Brook M A and Brennan J D 2004 Fluorescence anisotropy studies of solute interactions with covalently modified colloidal silica nanoparticles Langmuir **20** 848-854

[11] Laursen Bo W, Krebs F C 2001 Synthesis, Structure, and Properties of Azatriangulenium Salts Chemistry – A European Journal **7** 1773-1783

[12] Sørensen T J, Thyrhaug E, Szabelski1 M, Luchowski R, Gryczynski1 I, Gryczynski1 Z, Laursen Bo W 2013 Azadioxatriangulenium: a long fluorescence lifetime fluorophore for large biomolecule binding assay Methods Appl. Fluoresc. 1 025001. doi:10.1088/2050-6120/1/2/025001.

[13] Thyrhaug E, Sørensen T J, Gryczynski I, Gryczynski Z and Laursen B W 2013 Polarization and Symmetry of Electronic Transitions in Long Fluorescence Lifetime Triangulenium Dyes J. Phys. Chem. A 117 2160–2168

[14] Cummins B, Simpson J, Gryczynski Z, Sørensen T J, Laursen Bo W, Graham D, Birch D, Coté G. 2014 ConA-based glucose sensing using the long-lifetime Azadioxatriangulenium fluorophore. Proc. SPIE **8951**, Optical Diagnostics and Sensing XIV: Toward Point-of-Care Diagnostics, 89510A; doi: 10.1117/12.2039824

[15] Rich, R M, Mummert M, Gryczynski Z, Borejdo J, Sørensen T J, Laursen Bo W, Foldes-Papp Z, Gryczynski, I and Fudala, R 2013 Elimination of autofluorescence in fluorescence correlation spectroscopy using the AzaDiOxaTriAngulenium (ADOTA) fluorophore in combination with time-correlated single-photon counting (TCSPC) Analytical and Bioanalytical Chemistry **405** 4887-4894.

[16] Chib, R, Raut S, Shah S, Grobelna B, Akopova I, Rich R, Sørensen T J, Laursen Bo W, Grajek H, Gryczynski Z, Gryczynski I 2015 Steady state and time resolved fluorescence studies of azadioxatriangulenium (ADOTA) fluorophore in silica and PVA thin films Dyes and Pigments **117**, 16-23.

[17] Heilemann M, van de Linde S, Schüttpelz, Kasper R, Seefeldt B, Mukherjee A, Tinnefeld P, Sauer M 2008 Subdiffraction-resolution fluorescence imaging with conventional fluorescent probes Angew. Chem. Int. Ed. **47**, 6172-6176.

[18] Erdelyi M, Rees E, Metcalf D, Kaminski-Schierle G S, Dudas L, Sinko J, Knight A E and Kaminski C F 2013 Correcting chromatic offset in multicolor super-resolution localization microscopy Optics Express **21**(9)10978-10988

[19] Steiner R F 1991 Fluorescence anisotropy: Theory and applications Topics in Fluorescence Spectroscopy: Principles (vol 2) ed J. R. Lakowicz, (New York: Plenum Press) 1-51

[20] Weber G 1952 Polarization of the fluorescence of macromolecules - 1. Theory and experimental method Biochem. J. **52** 145-155.

[21] Smith T and Ghiggino K 2015 A review of the analysis of complex time-resolved fluorescence anisotropy data Methods Appl. Fluoresc. **3** 022001 doi:10.1088/2050-6120/3/2/022001

[22] Birch D J S and Yip P Nanometrology 2014 Fluorescence spectroscopy and microscopy: methods and protocols. Eds. Y Engelborghs and T Visser. Vol. 1076 Methods in Molecular Biology. Humana Press. Ch.11, 279-302. doi 10.1007/978-1-62703-649-8_11

[23] Rees E J, Erdelyi M, Kaminski-Schierle G S, Knight A E and Kaminski C F 2013 Elements of image processing in localisation microscopy Journal of Optics **15** 094012

[24] Metcalf D J, Edwards R, Kumarswami N and & Knight A E 2013 Test Samples for Optimizing STORM Super-Resolution Microscopy Journal of Visualized Experiments **79** e50579

[25] Geddes C D, Apperson K and Birch D J S 2000 New fluorescent quinolinium dyes - applications in nanometre particle sizing Dyes Pigm. 44, 69-74.

[26] Karolin J and Geddes C D 2015 Silica nanoparticle metrology using URSA Blue and colloidal Ludox solutions Dyes Pigm. **112**, 50-53.

[27] Buckley A M and Greenblatt M 1994 The sol-gel preparation of silica gels J. Chem. Ed. **71**, 599-602.

[28] Green D L, Lin J S, Lam Y F, Hu M Z-C Schaefer D W, Harris M T 2003 Size, volume fraction, and nucleation of Stober silica nanoparticles. J. Coll. Int. Sci. **266** 346-358.

[29] Bogh S A, Bora I, Rosenberg M, Thyrhaug E, Laursen Bo W and Sørensen T J 2015 Azadioxatriangulenium: exploring the effect of a 20 ns fluorescence lifetime in fluorescence anisotropy measurements Methods Appl. Fluoresc. 3 045001 doi.org/10.1088/2050-6120/3/4/045001

[30] Dempsey G T, Vaughan J C, Chen K H, Bates M and Zhuang X 2011 Evaluation of fluorophores for optimal performance in localization-based super-resolution imaging Nature Methods **8**, 1027–1036 doi:10.1038/nmeth.1768

[31] Spahn C, Cella-Zannacchi F, Endesfelder U and Heilemann M 2015 Correlative super-resolution imaging of RNA polymerase distribution and dynamics, bacterial membrane and chromosomal structure in Escherichia coli. Methods Appl. Fluoresc. **3** 014005 doi:10.1088/2050-6120/3/1/014005